Enhanced Electro-Optic Phase Shifts in Suspended Waveguides

T. H. Stievater,[1] D. Park,[1] W. S. Rabinovich,[1] M. W. Pruessner,[1], S. Kanakaraju,[2] C. J. K. Richardson,[2] and J. B. Khurgin[3]

[1]*Naval Research Laboratory, Washington, DC 20375*
[2]*Laboratory for Physical Sciences, College Park, MD 20740*
[3]*Johns Hopkins University, Baltimore, MD 21218*
Email: opticalmems@nrl.navy.mil

Abstract: We demonstrate enhanced electro-optic phase shifts in suspended InGaAs/InGaAsP quantum well waveguides compared to attached waveguides. The enhancement stems from an improved overlap between the optical mode and the multiple quantum well layers in thin waveguides when the semiconductor material beneath the waveguide is selectively etched. The measured voltage length product is 0.41 V-cm and the measured propagation loss is 2.3 ± 0.7 dB/cm for the TE mode in the optical L-band.

OCIS codes: (160.6000) Semiconductors, including MQW; (230.3990) Microstructure devices; (160.2100) Electro-optical materials

References and links

1. T. H. Stievater, W. S. Rabinovich, P. G. Goetz, R. Mahon, and S. C. Binari, "A Surface-Normal Coupled-Quantum-Well Modulator at 1.55 Microns," IEEE Photon. Technol. Lett. (**16**), 2036–2038 (2004).
2. E. Kunkee, C.-C. Shih, Q. Chen, C.-J. Wang, and L. J. Lembo, "Electrorefractive Coupled Quantum Well Modulators: Model and Experimental Results," IEEE J. Quantum Electron. (**43**), 641–650 (2007).
3. J. Shin, S. Wu, and N. Dagli, "Bulk Undoped GaAs–AlGaAs Substrate-Removed Electrooptic Modulators With 3.7-V-cm Drive Voltage at 1.55 μm," IEEE Photon. Technol. Lett. (**18**), 2251–2253 (2006).
4. J. Shin, Y.-C. Chang, and N. Dagli, "0.3 V drive voltage GaAs/AlGaAs substrate removed Mach–Zehnder intensity modulators," Appl. Phys. Lett. (**92**), 201,103–201,105 (2008).
5. T. H. Stievater, W. S. Rabinovich, D. Park, J. B. Khurgin, S. Kanakaraju, and C. J. K. Richardson, "Low-loss suspended quantum well waveguides," Opt. Express (**16**), 2621–2627 (2008).
6. D. Park, T. H. Stievater, W. S. Rabinovich, N. Green, S. Kanakaraju, and L. C. Calhoun, "Characterization of hydrogen silsesquioxane as a Cl_2/BCl_3 inductively coupled plasma etch mask for air-clad InP-based quantum well waveguide fabrication," J. Vac. Sci. Technol. B. (**24**), 3152–3156 (2006).
7. R. J. Deri and E. Kapon, "Low-loss III-V semiconductor optical waveguides," IEEE J. Quantum Electron. (**27**), 626–640 (1991).
8. S. Pogossian, L. Vescan, and A. Vonsovici, "The single-mode condition for semiconductor rib waveguides with large cross section," J. Lightwave. Technol. (**16**), 1851–1853 (1998).
9. T. Ikegami, "Reflectivity of mode at facet and oscillation mode in double-heterostructure injection lasers," IEEE J. Quantum Electron. (**8**), 470 (1972).
10. P. C. Kendall, D. A. Roberts, P. N. Robson, M. J. Adams, and M. J. Robertson, "New formula for semiconductor laser facet reflectivity," IEEE Photon. Technol. Lett. (**5**), 148–150 (1993).
11. E. M. Skouri, P. Martin, L. Chusseau, C. Alibert, C. Coriasso, D. Campi, and C. Cacciatore, "Measurement of the refractive index of GaInAs/InP quantum wells by a grating coupling technique," Appl. Phys. Lett. (**67**), 3441–3443 (1995).
12. S. Nishimura, H. Inoue, H. Sano, and K. Ishida, "Electrooptic effects in an InGaAs/InAlAs multiquantum well structure," IEEE Photon. Technol. Lett. (**4**), 1123–1126 (1992).
13. J. E. Zucker, *Properties of Lattice-Matched and Strained Indium Gallium Arsenide*, in EMIS Datareviews (INSPEC, 1993). (and references contained therein).
14. S. Adachi, *Physical properties of III-V semiconductor compounds: InP, InAs, GaAs, GaP, InGaAs, and InGaAsP* (Wiley-VCH, 1992).

#119157 - $15.00 USD Received 27 Oct 2009; revised 17 Dec 2009; accepted 17 Dec 2009; published 6 Jan 2010

Report Documentation Page

Form Approved
OMB No. 0704-0188

1. REPORT DATE	2. REPORT TYPE	3. DATES COVERED
2010		**00-00-2010 to 00-00-2010**

4. TITLE AND SUBTITLE	5a. CONTRACT NUMBER
Enhanced Electro-Optic Phase Shifts in SuspendedWaveguides	5b. GRANT NUMBER
	5c. PROGRAM ELEMENT NUMBER
6. AUTHOR(S)	5d. PROJECT NUMBER
	5e. TASK NUMBER
	5f. WORK UNIT NUMBER
7. PERFORMING ORGANIZATION NAME(S) AND ADDRESS(ES) **Naval Research Laboratory,Washington,DC,20375**	8. PERFORMING ORGANIZATION REPORT NUMBER
9. SPONSORING/MONITORING AGENCY NAME(S) AND ADDRESS(ES)	10. SPONSOR/MONITOR'S ACRONYM(S)
	11. SPONSOR/MONITOR'S REPORT NUMBER(S)

12. DISTRIBUTION/AVAILABILITY STATEMENT
Approved for public release; distribution unlimited

13. SUPPLEMENTARY NOTES

14. ABSTRACT

15. SUBJECT TERMS

16. SECURITY CLASSIFICATION OF:			17. LIMITATION OF ABSTRACT	18. NUMBER OF PAGES	19a. NAME OF RESPONSIBLE PERSON
a. REPORT	b. ABSTRACT	c. THIS PAGE			
unclassified	**unclassified**	**unclassified**	**Same as Report (SAR)**	**8**	

15. J. Mendoza-Alvarez, L. Coldren, A. Alping, R. Yan, T. Hausken, K. Lee, and K. Pedrotti, "Analysis of depletion edge translation lightwave modulators," J. Lightwave. Technol. (**6**), 793–808 (1988).
16. Q. Lu, W. Guo, D. Byrne, and J. F. Donegan, "Design of Low V_π High-Speed GaAs Travelling-Wave Electrooptic Phase Modulators Using an n-i-p-n Structure," IEEE Photon. Technol. Lett. (**20**), 1805–1807 (2008).

1. Introduction

Compound-semiconductor-based electro-optic modulators are poised to displace lithium niobate (LiNbO3) as the material of choice for applications that require modulation voltages (the so-called V_π) $\ll$ 1 V. Such applications include systems for microwave photonics, on-chip interconnects, and ultra-high frequency modulators. For example, in microwave photonics, arrays of modulators have been proposed to simultaneously encode multiple microwave signals onto an optical carrier. RF power scaling dictates that these systems use modulators that operate at the lowest possible V_π, ideally much less than one volt. To reduce V_π, compound semiconductor heterostructures such as coupled quantum wells [1, 2] enable the enhancement of electro-optic coefficients at wavelengths near the material bandedge. In addition, compound semiconductor heterostructures enable the design of waveguides that confine the optical mode between two closely spaced electrode layers, reducing the voltage needed to achieve a large electric field. This second advantage can be further extended by removing the semiconductor material from above and below the waveguide, providing the tightest possible out-of-plane optical confinement by maximizing the index contrast in that dimension. In fact, such a substrate removal technique has previously been reported [3, 4] in the GaAs/AlGaAs system, with a reported drive voltage length product of 0.21 V cm. The substrate removal was achieved using a low-index transfer substrate that allowed complete etching of the GaAs substrate beneath the waveguide.

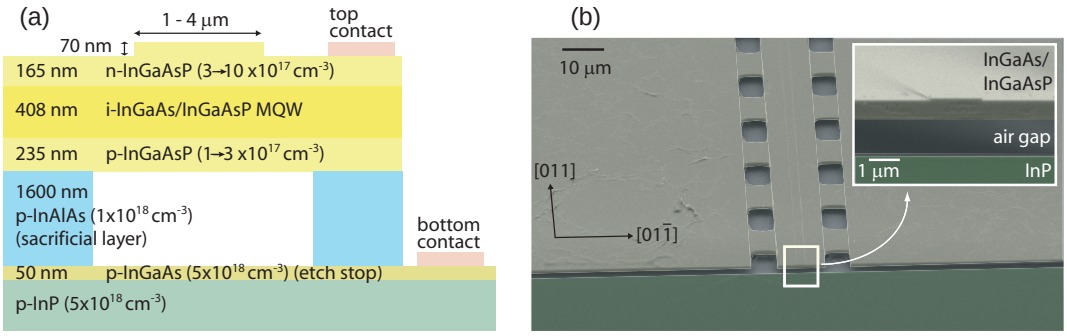

Fig. 1. **(a)**: The epitaxial layer structure and waveguide rib dimensions (not to scale). **(b)**: A false-color SEM image of a suspended quantum well waveguide comprised of a shallow rib bounded by etch holes, prior to the deposition of the metal contacts. Inset: the facet of a 2 μm wide rib.

In this work, we report on a novel process that uses surface micromachining to remove the semiconductor material beneath InGaAs/InGaAsP multiple quantum well (MQW) waveguides grown on an InP substrate [5]. By growing the quantum well waveguides on a InAlAs sacrificial layer, a simple selective etch suspends the waveguides in air for high-index confinement in the out-of-plane direction. Since the InAlAs sacrificial layer has a lower refractive index than the waveguide, we can compare the electro-optic phase shift before and after this layer is selectively etched. This comparison demonstrates that suspending the MQW waveguides results in tighter optical mode confinement and enhanced electro-optic phase shifts.

#119157 - $15.00 USD Received 27 Oct 2009; revised 17 Dec 2009; accepted 17 Dec 2009; published 6 Jan 2010

2. Fabrication

The waveguides are comprised of a 32-period $In_{.48}Ga_{.52}As/In_{.82}Ga_{.18}As_{.40}P_{.60}$ MQW that is grown between two partially doped 235 nm thick InGaAsP layers, forming a p-i-n diode. A structure schematic is shown in Fig. 1. The first 20 nanometers of the bottom InGaAsP layer immediately below the MQW is undoped, followed by p-doping that is graded from 1×10^{17} cm^{-3} to 3×10^{17} cm^{-3} at the sacrificial layer. Similarly, the first 20 nanometers of the top InGaAsP layer is undoped, followed by n-doping that is graded from 3×10^{17} cm^{-3} to 10×10^{17} cm^{-3} at the waveguide top. This 880 nm thick waveguide layer is grown on a p-InAlAs sacrificial layer using molecular beam epitaxy. The MQW is designed to have a heavy-hole band edge at approximately 1475 nm, allowing for operation in the optical L-band [5]. The waveguides are designed to have a phosphorus fraction in any layer below 0.65 to prevent etching during exposure to the HCl:H2O (3:1) selective etch. The sample is etched for approximately 15 minutes, which results in lateral etching of the InAlAs of approximately 20 μm. In addition, the waveguide alloy fractions were chosen such that the waveguide would have a small amount of net tensile strain to ensure flatness upon release from the sacrificial layer: too much tensile strain and the material cracks, whereas even small amounts of compressive strain induce buckling in the suspended material.

The 1-4 μm wide waveguide ribs are fabricated in both the [011] and [$0\bar{1}1$] directions using electron-beam lithography and plasma etching [6]. As shown in Fig. 1, the rib is etched to a depth of approximately 70 nm, enabling operation at the fundamental waveguide mode for both TM and TE polarized light. A second lithography step is used to etch holes alongside the waveguides to a depth that penetrates into the InAlAs sacrificial layer. These holes are spaced either 5 μm or 10 μm from the waveguide edge, a distance chosen to enable release of the waveguides from the sacrificial layer upon exposure to the selective HCl etch without degrading the waveguide transmission. Finally, metal contacts are deposited on both the top n-InGaAsP layer and on the p-InGaAS etch stop layer so that a reverse bias results in a vertical (out-of-plane) electric field across the MQW. The waveguides are cleaved to lengths between 2.4 mm and 7.2 mm and the facets are left uncoated.

3. Optical Loss

Optical loss and electro-optical phase shift measurements are made for the waveguides both prior to and after the selective etch step. Fig. 1 shows one particular waveguide after the selective etch step, clearly showing that the waveguides are suspended in air. Tunable polarized laser light is coupled into and out of the waveguides using a high numerical-aperture nanopositioning system. The Fabry-Perot fringes formed by reflections from the waveguide end-facets are analyzed to provide a measurement of the fringe contrast (K), phase shift ($\Delta\phi^{(FP)}$), and free-spectral-range (FSR) as a function of reverse bias, polarization, and wavelength for a given waveguide. The contrast of the Fabry-Perot fringes is used to estimate the losses incurred during propagation between the end facets [7]. The change of the fringe phase as a function of reverse bias is a measurement of the strength of the electro-optic effect. Last, The FSR is a measurement of the group index, which provides a check that only the fundamental mode for a given polarization is excited. In fact, wider waveguides (4 μm and above) do show evidence of propagation of higher-order modes, consistent with our modal calculations [8]. These waveguides are not used in our loss analysis or electro-optic analysis.

Fig. 2 shows a plot of the quantity $\ln(1-\sqrt{1-K^2})-\ln(K)$ vs. the waveguide length, for wavelengths of 1600 nm and 1620 nm. The data points represent an average found across a range of waveguides of equal length at these two wavelengths, and the error bars represent the standard error associated with this average. Plotted in this way, the y-intercept is $\ln(R)$ where R is the facet reflectivity, and the slope is the propagation loss, α, in cm^{-1}. A least-squares fit

#119157 - $15.00 USD Received 27 Oct 2009; revised 17 Dec 2009; accepted 17 Dec 2009; published 6 Jan 2010

to the data gives a TE propagation loss of 2.3±0.7 dB/cm, a TE facet reflectivity of 0.36±0.02, a TM propagation loss of 1.8±1.7 dB/cm, and a TM facet reflectivity of 0.18±0.02. The polarization dependence of the facet reflectivity is due to the asymmetry of the subwavelength mode [9, 10], and can be estimated from

$$R_{TE(TM)} = R_0(1+(-)(k_y^2-k_x^2)+(k_y^4+k_x^4)) \quad (1)$$
$$k_i = \frac{\sqrt{\ln 2/n_{eff}}\lambda}{\pi a_i}$$

where R_0 is the Fresnel reflectivity (here 0.28), λ is the wavelength, n_{eff} is the effective modal index, and a_i is the full-width-at-half-maximum of the mode in that dimension. For the fundamental TE mode, the calculated facet reflectivity is 0.39, whereas for the fundamental TM mode the calculated reflectivity is 0.23, in qualitative agreement with our measurements. In addition, comparison of loss among waveguides of various widths with the same length shows that the loss is independent of waveguide width for widths as small as 1.5 μm, implying that sidewall roughness is not a dominant source of loss within this waveguide width range. In addition, above 1580 nm, the loss is independent of wavelength, which indicates that near-bandedge absorption is also not a limiting loss factor in this wavelength range. We do observe a much larger loss in these waveguides before the sacrificial layer is removed: approximately 15 dB/cm for both polarizations. Since the sacrificial layer is p-doped at $\sim 1\times10^{18}$ cm^{-3}, we believe that free-carrier absorption at even this moderate p-doping level contributes significantly to this propagation loss.

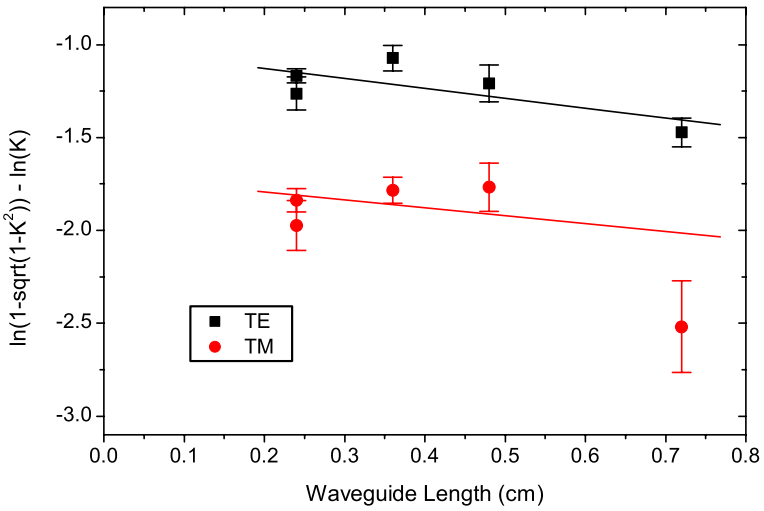

Fig. 2. Fabry-Perot method for measuring propagation loss in the suspended waveguides. The lines are least-square fits to the data.

4. Electro-optical properties

The electro-optic effect in a waveguide geometry induces a change in the optical phase, $\Delta\phi$:

$$\Delta\phi = 2\pi L\Delta n/\lambda \quad (2)$$

#119157 - $15.00 USD Received 27 Oct 2009; revised 17 Dec 2009; accepted 17 Dec 2009; published 6 Jan 2010

where L is the waveguide length, Δn is the change in the refractive index, and λ is the free-space wavelength. In a zinc-blende semiconductor, Δn is comprised of contributions from both the linear (Pockels) effect and the quadratic (Kerr) effect for the TE mode, whereas for the TM mode it arises exclusively from the quadratic effect:

$$\Delta n_{TM} = -n^3 s_{11} E^2 \Gamma_{TM}/2 \quad (3)$$

$$\Delta n_{TE}^{[011]} = -n^3 (s_{12} E^2 + r_{41} E) \Gamma_{TE}/2 \quad (4)$$

$$\Delta n_{TE}^{[0\bar{1}1]} = -n^3 (s_{12} E^2 - r_{41} E) \Gamma_{TE}/2 \quad (5)$$

$$\Delta n_{TE}^{[001]} = -n^3 s_{12} E^2 \Gamma_{TE}/2 \quad (6)$$

where n is the refractive index, r_{41} is the linear electro-optic tensor component, s_{11} is the diagonal component of the quadratic electro-optic tensor (which here arises primarily from the light-hole quantum-confined Stark effect), s_{12} is the off-diagonal component of the quadratic electro-optic tensor (which here arises primarily from the heavy-hole quantum-confined Stark effect), E is the electric field (negative for our definition of coordinate axes), and Γ is the overlap factor between the electric field or the square of the electric field and the optical mode. In this work we use the abrupt-junction approximation to estimate the depletion width and thus the electric field strength. Note that the electric field is the sum of the built-in junction voltage and the external reverse bias. Separate measurements (not shown) confirm that the TM electro-optic effect is independent of the waveguide direction, whereas the TE effect is strongest in the [011] direction and weakest in the [$0\bar{1}1$] direction. The quadratic effect is significant for our measurements since we operate close to the MQW bandgap, where the quantum-confined Stark effect is strongest. Note that it is the Γ terms that account for the bulk of the enhancement of the phase shift when the waveguides are suspended; a suspended waveguide has a smaller out-of-plane optical mode than an attached waveguide, which improves the overlap with the thin MQW layer.

The electro-optic phase shift is measured by monitoring the Fabry-Perot fringes formed by reflections from the end facets while a reverse voltage is applied to the waveguide. The phase shift measured in this way is equivalent to a push-pull phase shift in a Mach-Zehnder electro-optic modulator with arms of length equal to our waveguide length. Thus, the measured Fabry-Perot phase shift for a given waveguide length, $\Delta\phi^{(FP)}$, is twice the phase shift of Eq. 2, $\Delta\phi$.

The phase of these Fabry-Perot fringes (with respect to the phase at 0 V bias) for 1600 nm and 1620 nm in a 4.8 mm long [011]-oriented waveguide prior to and after release is plotted in Fig. 3a for TE polarized light and in Fig. 3b for TM polarized light. Similar results are observed for other waveguides on the sample. As expected, the TE phase shift is larger than the TM phase shift. Both polarizations show a clear enhancement in the phase shift of suspended waveguides compared to attached waveguides for voltages up to 1 V. For voltages above 1 V, the p-doped InGaAsP contact layer begins to fully deplete, and the field across the MQW in the waveguide saturates. The inset in Fig. 3 shows the Fabry-Perot fringes from transmission spectra at 0 V and 0.85 V that are used to measure the phase shift at 1620 nm. The phase shift is measured for wavelengths between 1580 nm and 1640 nm. Within this wavelength range, the additional propagation loss incurred due to the applied voltage is small ($<$ 1.5 dB at 1 V reverse bias at 1580 nm). However, this additional loss during reverse bias for the TE mode for wavelengths below 1580 nm becomes significant due to the red-shift of the band edge.

For wavelengths between 1580 nm and 1640 nm, the overall measured TE phase-shift enhancement factor averages 1.19 with a maximum value of 1.28 at 1640 nm. The measured TM enhancement is between 1.41 and 1.52, with an average of 1.44. This enhancement factor is almost entirely due to the increase of the overlap factors before and after waveguide release, $\Gamma^{suspended}/\Gamma^{attached}$, with only a small contribution from changes to the modal index. The en-

#119157 - $15.00 USD Received 27 Oct 2009; revised 17 Dec 2009; accepted 17 Dec 2009; published 6 Jan 2010

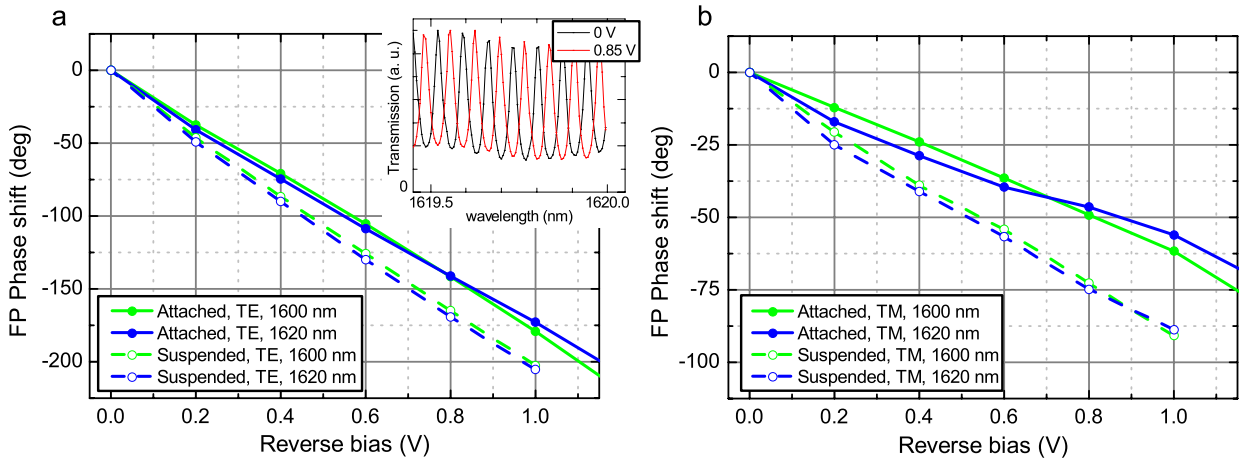

Fig. 3. Measured Fabry-Perot phase shift vs. reverse bias for TE (**a**) and TM (**b**) light in the optical L-band. Inset: The TE Fabry-Perot fringes for reverse biases of 0 V and 0.85 V.

hancement is larger for the TM mode than for the TE mode because the boundary conditions for the TM mode allow the optical field to be discontinuous across the upper and lower waveguide boundary. This permits more of the TM field to be confined within the waveguide in high-index-contrast structures that are $\sim \lambda$ thick.

To calculate this enhancement, we use a wavelength-dependent refractive index function [11] for an InGaAs-based MQW that has only two free-parameters: the light-hole and heavy-hole band edges. This refractive index is combined with a finite-element mode solver to estimate the integrated TE and TM mode power confined between the waveguide contact layers, for waveguides on a material with $n = n_{InAlAs}$ (attached) or $n = 1$ (suspended). This technique has previously been used to accurately compare our measured group velocity with the calculated group velocity in tightly confined suspended MQW waveguides [5]. Our model predicts an average TE enhancement of 19% between 1580 nm and 1640 nm, which agrees with our measured enhancement, and is primarily due to improved modal overlap with the MQW (e. g. $\Gamma_{TE}^{suspended}/\Gamma_{TE}^{attached}$ = 0.74/0.63 at 1620 nm). The predicted average TM enhancement is 37% (e. g. $\Gamma_{TM}^{suspended}/\Gamma_{TM}^{attached}$ = 0.79/0.60 at 1620 nm), only slightly lower than our average measured value.

Fig 4 shows the TE Fabry-Perot phase shift in the suspended [011]-oriented waveguides for wavelengths from 1580 nm to 1640 nm. The phase shift is relatively constant and linear within this wavelength range, even though the wavelength is only 100 nm to 160 nm from the band edge. This is most likely due to the fact that at external voltages less than 1 V, the contribution to the phase shift from the linear electro-optic effect (which is largely wavelength-independent) is larger than that of the quadratic effect. In fact, an expansion of Eq. 4 shows that the largest contribution from the s_{12} term at these voltages is actually linear in the *external* field and smaller than the r_{41} term: $s_{12}E_{ext}^2 < 2s_{12}E_{bi}E_{ext} < r_{41}E_{ext}$ [12]. In addition, for the wavelength range 1580 nm to 1640 nm, the V_π varies between 0.85 V and 0.91 V, which corresponds to a minimum voltage length product of 0.41 V-cm in a suspended waveguide. This value represents an order of magnitude improvement over typical LiNbO3 devices, and is only 2 times larger than the equivalent value reported in Ref. [4], despite the fact that our waveguides are about 3 times thicker.

By comparing the phase shift values for the TE mode for waveguides oriented in the [011]

#119157 - $15.00 USD Received 27 Oct 2009; revised 17 Dec 2009; accepted 17 Dec 2009; published 6 Jan 2010

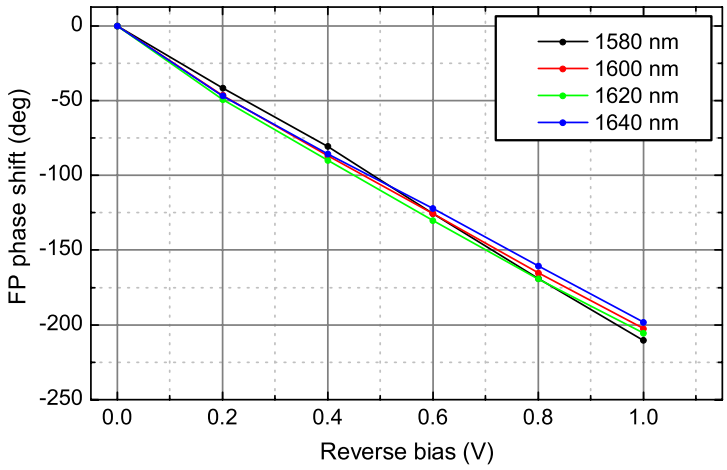

Fig. 4. Measured Fabry-Perot phase shift vs. reverse bias in a suspended [011] waveguide for the TE mode.

direction to those oriented in the [0$\bar{1}$1] direction, Eq. 4 and Eq. 5 can be used to estimate the values of r_{41} and s_{12} as a function of wavelength. Eq. 3 can also be used to estimate s_{11} from the measured TM phase change. The voltage-dependence of the depleted region, which is necessary to estimate the exact electric field at the quantum wells, is estimated from C-V measurements. These values of the electro-optic coefficients are shown in Fig. 5. Note that the error bars shown in this plot are dominated by the uncertainty in the exact depletion layer thickness, which we approximate using the abrupt-junction approximation. Our measured r_{41} is in the range of -1.0 pm/V to -1.8 pm/V, which is similar to previously reported values [12, 13, 14], which also range from -1.0 pm/V to -1.8 pm/V for InGaAs/InGaAsP-based structures. The apparent wavelength dependence of our measured r_{41} is likely an artifact that arises from our analysis technique: r_{41} is found from subtracting the phase shift data from two different samples, so that small absolute errors in the measured phase become large relative errors for r_{41}. This error would be the largest for wavelengths that show the largest overall phase shift (closest to the bandedge), implying that our most accurate r_{41} value is obtained furthest from the bandedge.

Our values for s_{11} and s_{12}, -2.8$\times 10^{-19}$ m^2/V^2 and -5.1 $\times$ 10^{-19} m^2/V^2 at 1580 nm, respectively, are lower than those previously reported for an InGaAs MQW [12]: -6.2$\times 10^{-19}$ m^2/V^2, and -15 $\times 10^{-19}$ m^2/V^2, respectively. However, our analysis of the data presented in Ref. [12] using their reported values of V_π and their Eq. 1 (equivalent to our Eqs. 3 and 4) shows an error in their calculations. The corrected values of s_{11} and s_{12} at 1580 nm from that work are -2.1$\times 10^{-19}$ m^2/V^2 and -5.8$\times 10^{-19}$ m^2/V^2, which are nearly identical to our values. It should be noted that in p-i-n semiconductor waveguide modulators, effects other than the linear and quadratic electro-optic effects, such as those related to a change in free-carrier distribution with voltage [15], can play an important role. Since these free-carrier based effects are direction-independent and approximately linear, they would be expected to appear in our analysis as linear contributions to Eqs. 3 through 6. However, our fitting to Eq. 3 (for s_{11}) and to the sum of Eqs. 4 and 5 (for s_{12}) shows excellent agreement with a model based on a purely quadratic effect, and the agreement of our values of s_{11} and s_{12} with that of previous reports together indicate that free-carrier effects do not play an important role in our measured phase-shifts.

#119157 - $15.00 USD Received 27 Oct 2009; revised 17 Dec 2009; accepted 17 Dec 2009; published 6 Jan 2010

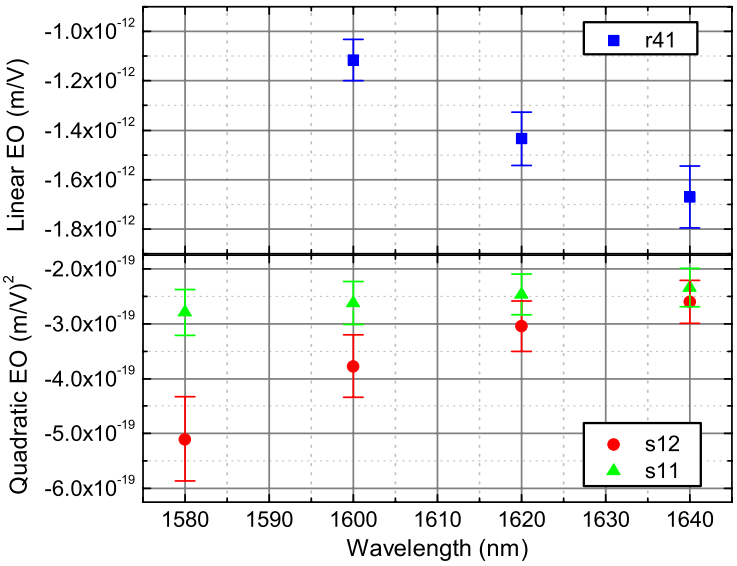

Fig. 5. Measured electro-optic tensor coefficients as a function of wavelength.

5. Conclusions

In this work, we have demonstrated that suspending electro-optic semiconductor waveguides reduces the voltage needed to achieve a π phase shift, resulting in a voltage-length product as low as 0.41 V-cm. Thinner waveguides will result in an even larger electro-optic phase shift by further increasing the electric field strength for a given voltage, with only a small decrease in the modal overlap factor. Such waveguides need to be carefully designed, however, to maintain low resistivity in the thin doped layers. Since p-doped layers have a significantly lower mobility and higher optical loss than n-doped layers (for the same doping level), future designs are focused on the use of an n-p-i-n [16] junction instead of a p-i-n. Such layers also offer the possibility to incorporate high-electron-mobility layers, to further decrease the carrier mobility and improve the RF performance. In such a device, the net waveguide thickness could be decreased to a few hundred nanometers, resulting in a significantly lower modulation voltage. When combined with coupled or asymmetric multiple quantum wells, suspended quantum well waveguides should enable wideband electro-optic modulators in the optical C-band with $V_\pi \ll 1V$.

#119157 - $15.00 USD Received 27 Oct 2009; revised 17 Dec 2009; accepted 17 Dec 2009; published 6 Jan 2010